International Forum on Aeroelasticity and Structural Dynamics
IFASD 2019
June 10-13, 2019, Savannah, Georgia, USA

DESIGN AND OPTIMIZATION OF AN AEROSERVOELASTIC WIND TUNNEL MODEL

Johannes K.S. Dillinger[1*], Yasser M. Meddaikar[1], Jannis Lübker [1], Manuel Pusch[2] and Thiemo Kier[2]

[1] German Aerospace Center (DLR),
Institute of Aeroelasticity, 37073 Göttingen, Germany
* Johannes.Dillinger@DLR.de

[2] German Aerospace Center (DLR),
Institute of System Dynamics and Control, 82234 Weßling, Germany

Keywords: composite optimization, aeroservoelasticity, wind tunnel testing

Abstract: Combining passive and active load alleviation techniques, this paper presents the design, optimization, manufacturing and update of a flexible composite wind tunnel model.
Starting from the specification of an adequate wing and trailing edge flap geometry, passive, static aeroelastic stiffness optimizations for various objective functions have been performed in a first step. The second optimization step comprised a discretization of the continuous stiffness distributions, resulting in manufacturable stacking sequences.
In order to determine which of the objective functions investigated in the passive structural optimization complemented most efficiently with the projected active control schemes, the condensed modal finite element models were integrated in an aeroelastic model, involving a dedicated gust load alleviation controller. The most promising design was selected for manufacturing. Based on the dynamic identification of the model the finite element representation could be updated to conform to the measured eigenfrequencies. Eventually, a wind tunnel test campaign was conducted in November 2018, results of which are examined in separate reports.

1 INTRODUCTION

The work presented in this paper is hosted in the DLR *KonTeKst* project [1], which focusses on the development and analysis of configurations and technologies for emission and noise reduced short range aircraft. Part of the project focuses on the development and testing of an actively controlled flexible composite wing, aiming at a validation of active load alleviation techniques.
Passive means of load alleviation have been a subject of research for many years. In particular the identification of the manifold benefits attainable with composite materials has led to a considerable amount of research work in the past decades, starting in the late 70's with the work by Starnes Jr and Haftka [2], describing a weight minimization subject to combinations of buckling, strength, displacement and twist responses. The effect of bending torsion coupling [3], and non-symmetric laminates [4], were already investigated in the 80's, with a detailed overview of aeroelastic tailoring techniques in general provided by Shirk et al. [5]. Vanderplaats and Weisshaar provided an early overview on composite optimization techniques [6]. More recent aeroelastic tailoring works, including also the manufacturing aspects and constraints were given by Stodieck et al. [7], [8], [9] and Stanford et al. [10], [11], the latter one presenting an overview of the state-of-the-art.

In [12], [13] the author describes a composite stiffness optimization framework focusing on passive aeroelastic tailoring problems, a derivative of which was employed in the present work.

Gust load alleviation by active means also has been investigated intensively and is implemented in many aircraft as summarized, e.g., in [14]. One of the earliest examples of an aircraft incorporating active control to alleviate structural loads during gust encounter is the Lockheed C-5A [15]. On the C-5A aircraft, several control algorithms which command coordinated aileron deflections based on acceleration measurements have been evaluated greatly reducing the wing bending moment during gusts and maneuvers. In modern aircraft, active gust load alleviation has become an integral part allowing for cost savings in terms of fuel and maintenance [14] . To achieve a maximum overall aircraft performance, the gust load alleviation function needs to be considered already in early aircraft design phases [16]. To that end, a highly automated procedure for gust load alleviation controller design and tuning is required. This, however, can be challenging, especially in case of a large number of measurements or control surfaces are available for gust load alleviation, which is generally desired for a better gust load alleviation capability. To tackle this problem, promising control approaches as proposed in [17] or [18] propose to blend control inputs and/or measurement outputs and thereby reduce the control problem size. Combining the idea of blending inputs and outputs with the objective of isolating and damping aeroelastic modes which dominate the structural loads, according blending-based control approach are introduced, e.g., in [19] and [20], where the approach from [20] is applied here.

2 MODEL DESIGN

2.1 Previous Campaigns: Lessons Learned

In previous projects, experience was gained with the entire process ranging from the structural layout, static aeroelastic optimization for various objective functions, model manufacturing to eventually a wind tunnel test campaign. The tests mainly served as a test bench for the optimization process and the manufacturability of unconventional laminate stacking sequences. The wind tunnel employed in these campaigns was the DLR owned subsonic *Side Wind Tunnel Facility* (SWG) in Göttingen, Germany, featuring a test section of 2.4×1.6m (width×height) and a maximum free stream velocity of 60m/s.

Figure 1: Wind tunnel models in previous test campaigns.

The first model comprised an unswept wing of 1.0m span, 0.2m constant chord and a symmetric airfoil [21]. It was built in collaboration with the Technical University of Delft, featuring a composite layup optimized for maximum static tip deflection, Figure 1 (left).
A forward swept wing featuring 1.6m span and an average chord of 0.24m was tested in the second test campaign [22], Figure 1 (right). Also for this wing the objective function was to

maximize tip deflection, while being constrained to a maximum tip twist. Aeroelastic tailoring in this case allowed for a stiffness distribution suppressing the detrimental wash-in effect usually present in forward swept designs. Both wings were fully passive designs without trailing edge flaps or similar means.
Some very general lessons learned concerning the use and validity of measurement results from the previous experiments can be summarized as follows:

- aeroelastic experiments combine the uncertainties of structural, aerodynamic, and measurement disciplines.
- eliminating uncertainties is key to finding realistic explanations for aeroelastic effects.
- elimination of uncertainties can be achieved by
    - separating the disciplines in pre-tests where ideally only one discipline at a time is involved; this allows for the identification of effects that can only be generated by the discipline investigated.
    - keeping disciplines as simple and predictable as possible.

Concerning aerodynamics, it was seen that the behavior of the wind tunnel with freestream velocities larger than 40-50 m/s became somewhat unpredictable. The sources for possible errors are increasing freestream turbulence, quick heating-up of test section and freestream flow, as well as noise.
Concerning structural layout it was seen that:

- it is of utmost importance to gather and document as much information on the actual building process of the model as possible. This will allow for a meaningful update of the simulation models and thus the elimination of a major source of uncertainties.
- composite properties have to be determined anew ideally with every new material applied in the model.
- clamping the model at the root and attaching it to the balance can be a large source for uncertainties. This relates to the internal structure of the model itself, as well as the external structure required to transfer loads from the model to the balance.

One of the most prominent advancements to be addressed in *KonTeKst* as compared to previous projects was the consideration of flaps to investigate active load alleviation techniques. The additional complexity introduced by this again underlined the need to minimize uncertainties in the related aerodynamic and structure disciplines.

2.2 Model Specification

Based on the findings depicted in section 2.1, and in particular in order to reduce modeling complexity while focusing on an adequate finite element and aerodynamic representation, a rather simple wing layout was chosen over a complex shape, Figure 2. The span was set to the previously realized 1.6m of the forward swept wing, representing a viable compromise amongst aspect ratio, wing flexibility and the wind tunnel cross-sectional dimensions.

Two standard symmetric airfoils NACA 0012 and NACA 0015, with a relative thickness of 12% and 15% respectively, were preselected for application in the model. Considering a wing chord of 0.25m, 2D lift and drag polars for a Reynolds number range of ≈0.1e6 to 1.0e6 were computed for both airfoils, NACA 0012 and NACA 0015, Figure 3. For the lower Reynolds number both airfoils indicate a noticeably non-linear lift curve slope, which basically is a result of laminar separation bubbles on the upper surface and a forward running transition

location. As expected, the drag coefficients of the thicker NACA 0015 airfoil in most areas surpass the ones for the thinner NACA 0012 airfoil. On the other hand, maximum lift coefficients are higher for the NACA 0015, however noting that $C_{l\ max}$ is usually overestimated in *XFOIL*, so that only the relative distance between NACA 0012 and NACA 0015 should be considered here.
In favor of adequate space for sensor/actuator installation, but also to maintain a moderate aerodynamic behavior (higher $C_{l\ max}$) the NACA 0015 airfoil was chosen.

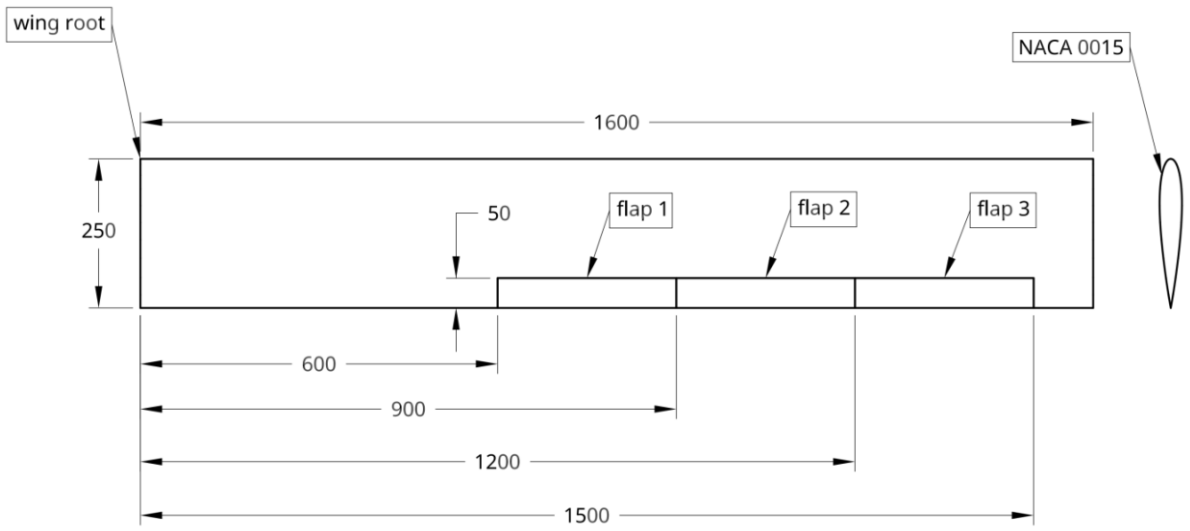

Figure 2: Wing geometry.

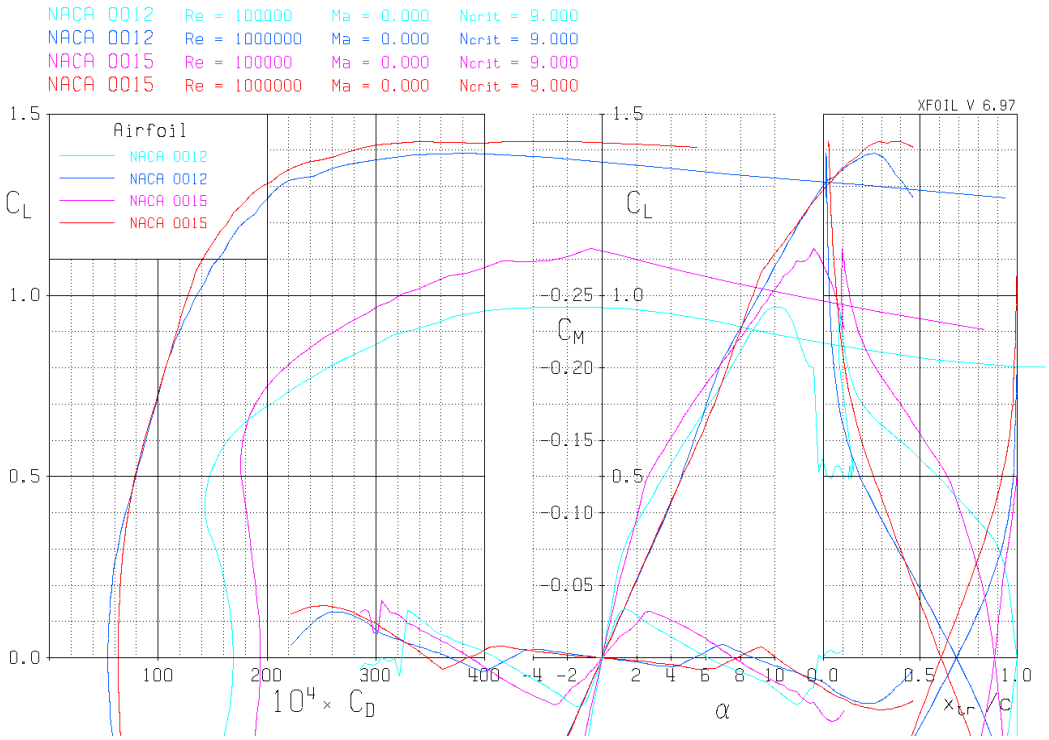

Figure 3: 2D polars for naca0012 and naca0015, free transition.

2.3 Flap Considerations

In order to estimate the capabilities of a regular camber changing trailing edge flap on the 3D wing, a *VSAERO* model was generated. To this end, *XFOIL* was used to generate airfoil coordinates for a flap featuring 20% relative flap depth and a deflection of 10° (positive downward), with the hinge line being placed on the symmetry line of the airfoil. Simulating a single flap ranging from y = 1.2m to 1.5m, the un-flapped airfoil coordinates were used from 0.0 m to 1.19 m, and again from 1.51m up to the tip at 1.6m, thus providing a transition zone from un-flapped to the flapped airfoil of 1.0cm on both sides of the flap. Figure 4 depicts the flap region, including a representation of off-body streamlines and pressure contours on the surface for a representative angle of attack of 6.0°.

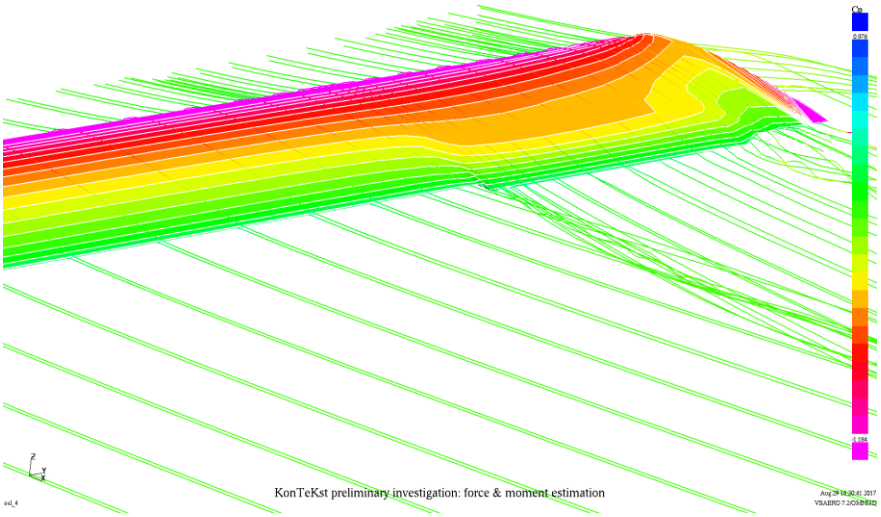

Figure 4: *VSAERO* model including a trailing edge flap ranging from y=1.2m to 1.5m.

In order to exploit the capabilities of an active flap system, also a more demanding flap architecture was investigated, as described in the following. Instead of one, three trailing edge flaps with a relative depth of 20 % were modelled, spanning approximately a region that on a standard-sized passenger aircraft would cover the trailing edge outside a possibly wing-mounted engine. Flap boundaries were chosen to be at y = 0.6 m, 0.9 m, 1.2 m, and 1.5 m. The outermost flap thus corresponds to the one investigated in the previous single flap case.

Table 1: Case definition for different flap combinations.

		case					
flap	spanwise boundaries	1	2	3	4	5	6
1	0.6m – 0.9m	0°	0°	0°	10°	0°	10°
2	0.9m – 1.2m	0°	0°	10°	0°	10°	10°
3	1.2m – 1.5m	0°	10°	0°	0°	10°	10°

Table 1 lists the different flap deflection cases investigated in the following. The flap deflection is again achieved by the application of appropriate airfoil coordinates, as generated with *XFOIL*. As in the single flapped case, static calculations for an alpha range of 0° to 10° and velocities from 10 m/s to 50 m/s were investigated. The relative change of lift force and root bending moment with respect to case 1 (no flap deflection) is plotted in Figure 5. Closely investigating the relative lift forces, plot on the left, reveals that a flap situated more towards the root is able to generate a larger lift force increase for a defined flap deflection than a flap

in the outer wing. This can be explained by means of the lift (circulation) distribution. While circulation and thus lift force as a result of pressure equalization tend towards zero at the tip, the effectiveness in increasing overall circulation by deflecting a flap is the highest in the area of highest circulation. In case of a rectangular, aerodynamically untwisted wing the circulation is the highest in the root. Thus, the closer a flap is positioned towards the root, the more effective it becomes in increasing lift.

The root bending moment on the other hand shows the opposite trend, the further outside the flap is located, the more additional root bending moment it can generate. Evidently, the increased lever arm dominates over the diminished lift force in the outer wing, meaning that a flap further outboard generates more root bending moment than an inboard flap, see Figure 5, plot on the right.
The calculations moreover indicates that combining flaps allows for a considerable increase in both, lift force and bending moment compared to single flap deflections. Depending on the optimization objective this can be a significant assistance in achieving the desired goals or in increasing the performance.

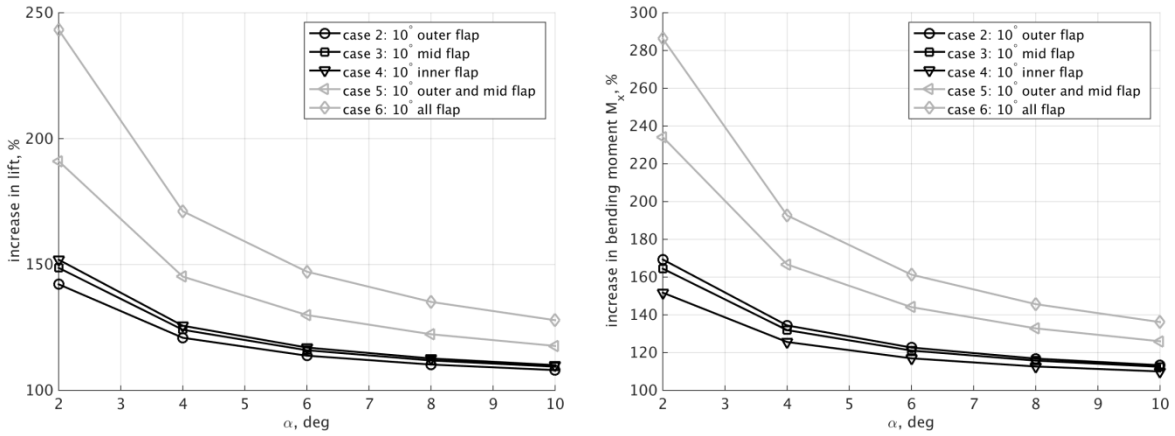

Figure 5: Relative increase of lift and root bending moment for various angles of attack (independent of flight velocity), and various flap deflection cases.

3 OPTIMIZATION

3.1 Analysis Model

The structural design was based on the experience gained in the first two wind tunnel campaigns. This involved the overall topological setup, as well as the employed materials. Regarding topology, a design with load carrying wing skins supported by a foam core was adapted. The material of choice for the wing skins was a unidirectional (UD) glass fiber with a surface weight of 220g/m^2. The main reason to prefer glass over carbon fiber were the higher strain allowables for the glass fiber and thus an increased flexibility of the wing. Moreover, the application of this material in previously tested wind tunnel models increased the confidence concerning its applicability.
First analysis models incorporated a dedicated shear web which later-on was removed by virtue of its negligible contribution to the overall performance, while noticeably increasing the constructional effort.

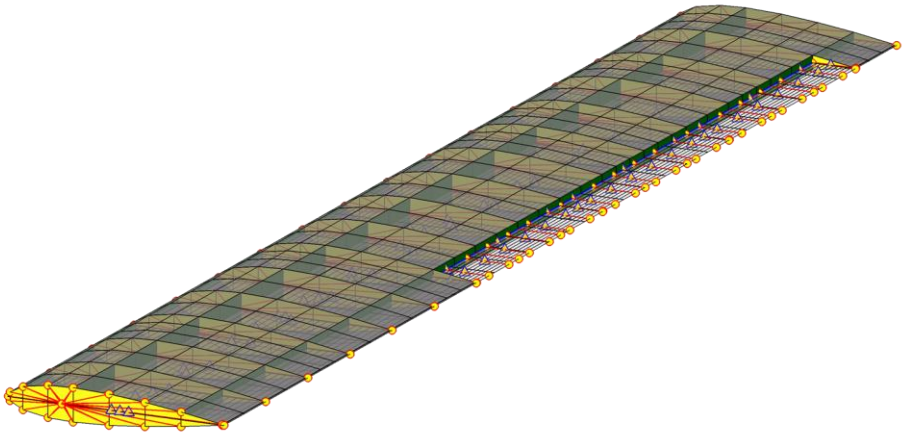

Figure 6: Wing finite element model.

The *Nastran* wing FE model was generated with the DLR in-house parametric modeling software *ModGen* [23], Figure 6. Again, based on experience gathered with previous wind tunnel models, the structural layout comprised load carrying composite skins and a foam core, represented in the FE model as shell and volume elements, respectively. *ModGen* also provided the doublet lattice (DLM) model as well as the coupling model for the interconnection of the structural and aerodynamic model.
Not being part of the optimization model, the flaps were modeled as beam rather than shell elements. To this end, a cross-sectional modeler was applied [24], providing among others a Timoshenko stiffness matrix, shear center location, mass matrix and the center of gravity location. The structural layout of the flap comprised a closed cell construction with carbon fiber skins on top and bottom, supported by a foam core. Closing of the cell was achieved by a glass fiber tube, which also served as a bearing for the rotational shafts making up the flap hinge. A representation of the spanwise constant cross-section as being defined for the cross-sectional modeler is shown in Figure 7. Each flap was hinged at three points, maintaining the rotational degree of freedom about the hinge axis. The pushrod connection suppressing the rotational motion was simulated by means of a spring attachment.

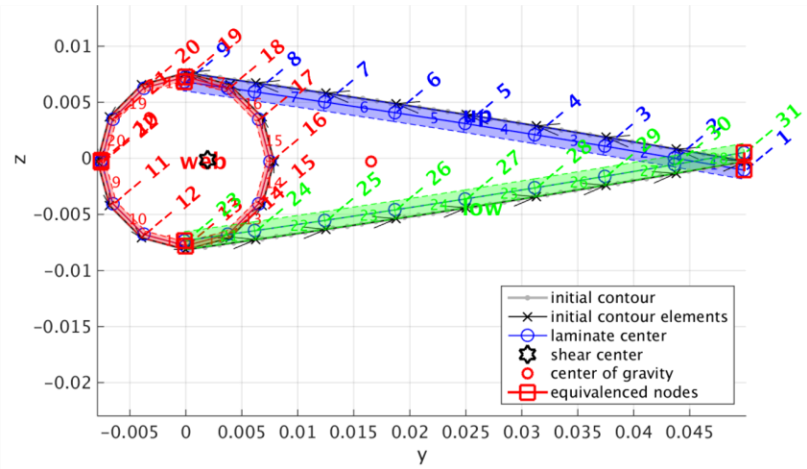

Figure 7: Flap cross-section.

In order to capture the dynamic behavior as accurate as possible, all masses known at this stage were considered in the finite element model. This incorporated structural data like the fiber volume fraction achievable in the envisioned manufacturing process and identified in

previously built models, as well as a precise representation of all non-structural masses like sensors (see Table 3), sensor mounting devices, sensor cabling, actuators and pushrods. Non-structural masses were modeled as point masses, attached via rigid body elements.

3.2 Structural Optimization

The wing skin layup was optimized in a two-step approach [13]. In a first step, the stiffness distribution represented as membrane and bending stiffness matrices was altered in dedicated design fields distributed in spanwise direction, a sample of which being shown in Figure 8. Serving as a sensible starting point, in a second step blended stacking sequences were optimized, eventually leading to layup tables directly suitable for the manufacturing process.

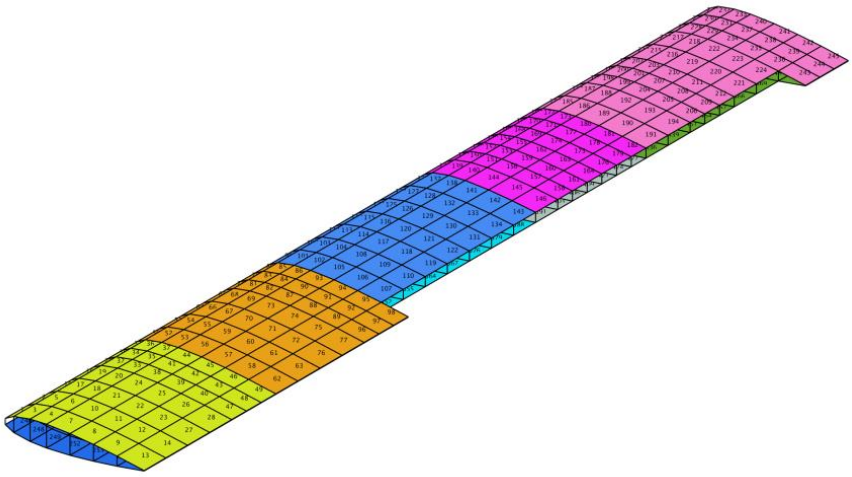

Figure 8: Design fields.

Responses considered in the optimization were mass, strain failure, aileron effectiveness, twist, displacement (both at the quarter chord and equidistant spanwise locations), divergence and eigenfrequencies. The load cases considered are listed in Table 2, where α is the angle of attack and **V** the free stream velocity. Load cases 1003 and 1006 were devoted to model sizing, representing the ultimate loads to be expected when running the wind tunnel at maximum velocity and considering a failure of the angle of attack adjustment.

Table 2: Optimization load cases.

case	type	α	V	flap 1	flap 2	flap 3
1001	α_{fixed}	5.0°	50.0 m/s	0.0°	0.0°	0.0°
1002	α_{fixed}	10.0°	50.0 m/s	0.0°	0.0°	0.0°
1003	α_{fixed}	15.0°	60.0 m/s	0.0°	0.0°	0.0°
1004	α_{fixed}	-5.0°	50.0 m/s	0.0°	0.0°	0.0°
1005	α_{fixed}	-10.0°	50.0 m/s	0.0°	0.0°	0.0°
1006	α_{fixed}	-15.0°	60.0 m/s	0.0°	0.0°	0.0°
1007	divergence	%	%	0.0°	0.0°	0.0°
1008	eigenfrequency	%	%	0.0°	0.0°	0.0°
1009	ail. eff.	%	50.0 m/s	0.0°	0.0°	1.0°
1010	ail. eff.	%	50.0 m/s	0.0°	1.0°	0.0°
1011	ail. eff.	%	50.0 m/s	1.0°	0.0°	0.0°

To identify which aeroelastic optimization objective would support most prominently the load alleviation controller, in total five objective functions were investigated in detail:

- aileron effectiveness maximization: η_{max}
- aileron effectiveness minimization: η_{min}
- tip deflection maximization: d_{max}
- tip deflection minimization: d_{min}
- 1st bending mode frequency minimization: f_{min}

It was seen that in case of the frequency minimization the optimizer simply increased the skin thickness in the outer wing, thereby introducing a large tip mass and consequently a decrease in eigenfrequency. To avoid this obvious, however unwished effect, but mainly to satisfy the lessons learned concerning a simple structural layout, the skin thickness eventually was fixed to 4×0.17mm=0.68mm throughout the skins, representing 4 layers of UD glass fiber.

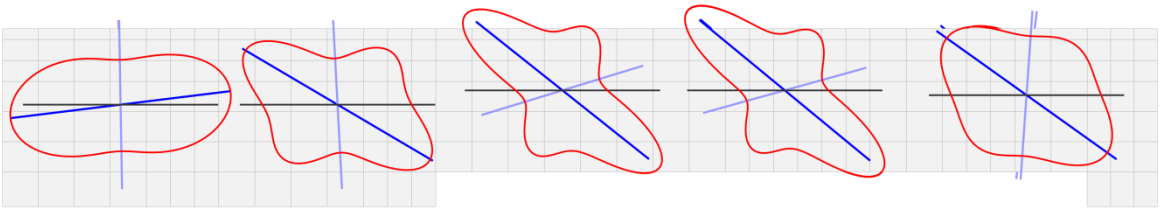

Figure 9: Optimized stiffness distribution $\hat{E}_{11}(\theta)$ for the η_{max} objective model.

The optimized stiffness distribution in the upper wing skin for the aileron effectiveness maximization objective is plotted in Figure 9, showing the polar thickness normalized engineering modulus of elasticity $\hat{E}_{11}(\theta) = 1/\hat{A}_{11}{}^{-1}(\theta)$, allowing for a visual assessment of the directional membrane stiffness distribution. It can be seen that in search of maximum aileron effectiveness, bending torsion coupling was introduced by tilting the main stiffness direction backward towards the tip. As a result, the twist towards the tip increases when bending the wing up (wash-in effect), thus augmenting the lift force for a downward (positive) flap deflection. Eventually, aileron effectiveness is increased.

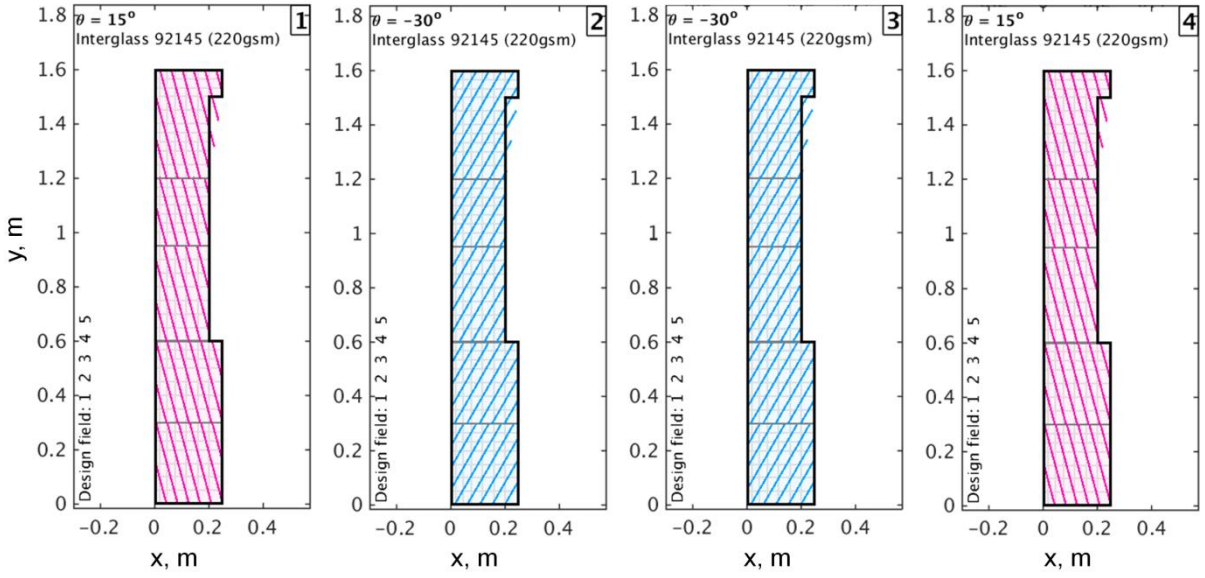

Figure 10: Stacking sequence for the η_{max} objective model.

As mentioned before, the second optimization step consisted of a stacking sequence retrieval based on the continuous result from step one [25]. Due to the definite specification of 4 layers and the constraints involved on laminate blending, the resulting stacking sequence design was simplified to 4 continuous layers present throughout the entire skin. The stacking sequence for the η_{max} objective is shown in Figure 10. The symmetric, unbalanced stack – identical for upper and lower skin – reflects the backward tilted main stiffness direction derived in optimization step one, Figure 9.

In order to reduce the number of degrees of freedom, a static Guyan reduction as provided in *Nastran* was applied. The models were condensed to 17 equally distributed grid points on the wing quarter chord, as well as 5 points along the hinge line of each flap. To validate the selection of reduced grid points, the so-called modal assurance criterion (MAC) matrix was computed for the full and the condensed model, Figure 11, showing a good agreement of the first 10 flexible modes.
The resulting mass and stiffness matrices could directly be implemented in the subsequent modal based controller design.

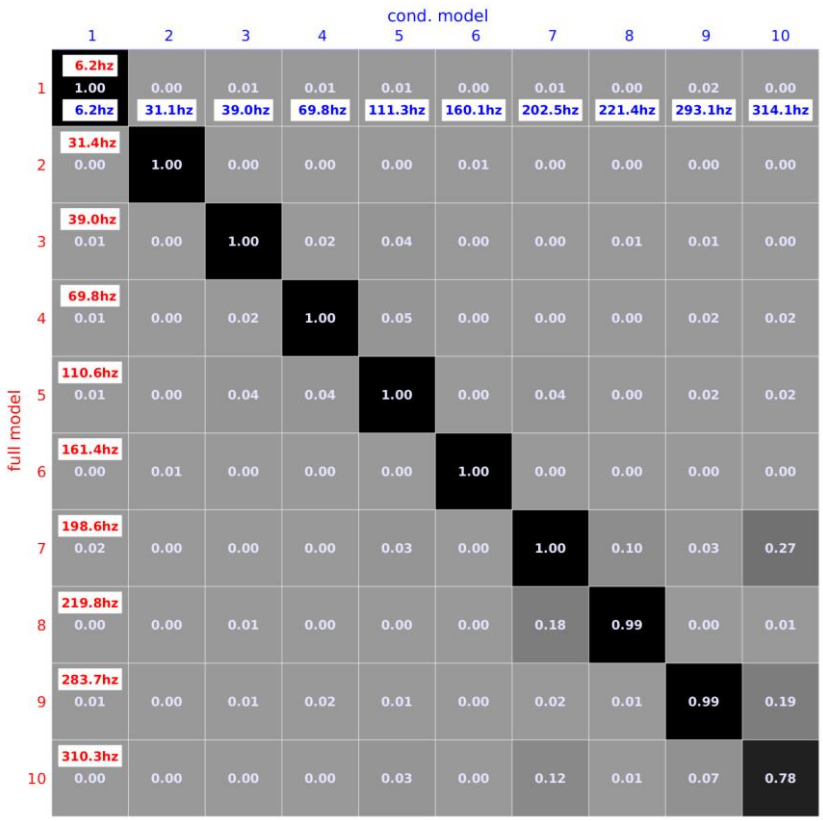

Figure 11: MAC matrix of full and condensed model

3.3 Controller Design and Model Selection

For each of the aeroelastically optimized models, a gust load alleviation controller was designed with the goal to maximize the wing root bending moment (WRBM) reduction. This means that the absolute value of the WRBM is of minor interest but rather the ratio of the WRBM with and without active gust load alleviation. The desired WRBM reduction was achieved by increasing the damping of the first wing bending mode, which clearly dominates

the WRBM. To that end, the modal control approach from [20] was applied, which proposes blending the control inputs and measurement outputs in an $\mathcal{H}_2$-optimal manner in order to isolate the target mode and enable a simplified single-input single-output (SISO) controller design. Here, the control inputs are the command signals for the servos driving the three trailing edge flaps and the measurement outputs are eight vertical accelerations measured at the outer part of the wing as depicted in Figure 12. As SISO controller, a proportional-integral (PI) controller was chosen. The respective proportional and integral gains were tuned as described in [26] and unified for all models since they vary only marginally. In contrast, the blending vectors were derived for each model, respectively. For more details on gust load alleviation controller design and tuning the reader is referred to [26].

To evaluate the achieved controller performance, a white noise vertical gust excitation was simulated by pitching the wing. For each model, the expected variance of the resulting WRBM with and without gust load alleviation controller was computed. Considering a true airspeed V_{TAS} = 40m/s for model selection, the corresponding WRBM reduction is depicted in Figure 13. It can be seen that the wing statically optimized for maximum aileron effectiveness yields the maximum load reduction of around 28% and hence, this model is selected for further evaluations.

In order to check if the required flap deflections are within limits, a harmonic pitching excitation at the natural frequency of the first wing bending mode was chosen as a worst-case excitation. At this frequency, the WRBM reduction of model 2 is 56% and the maximum flap deflection is 8° considering the maximum pitching amplitude of 5°. The largest flap deflections are well within the actuator limitations of $\pm$10° and occur at the outer flap, which was to be expected due to its maximum distance from the wing root.

Additionally, it has to be noted that distance of the first wing bending mode to the residual modes in terms of natural frequency is the largest for the aileron effectiveness optimized model. This is desirable since it implies reduced spillover effects, i.e. an undesired excitation of the residual modes, especially due to the limited actuator bandwidth. Based on all of these findings, the wing statically optimized for maximum aileron effectiveness was considered as best suitable for the wind tunnel test campaign and selected for manufacturing.

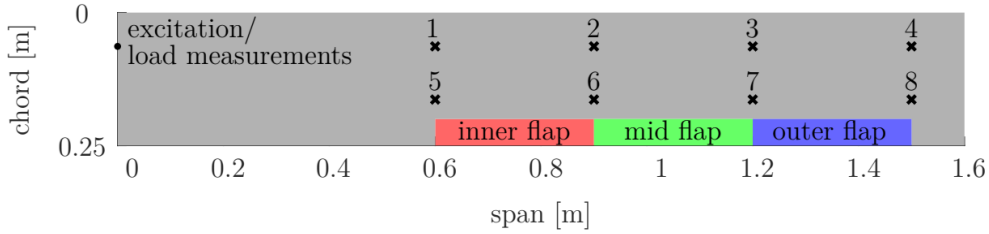

Figure 12: Position of flaps and sensors on the wing.

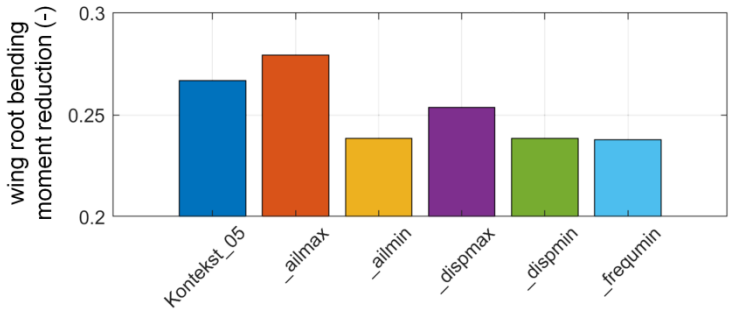

Figure 13: Comparison of the achieved WRBM reduction at V_{TAS} = 40m/s evaluated in terms of the expected variance for a white noise gust excitation simulated by pitching the wing.

4 MANUFACTURING AND UPDATE

4.1 Model-Building and Sensor Installation

Deciding in favor of the model optimized for maximum aileron effectiveness, the wing was manufactured in a three step procedure. First, the upper and lower wing skins were manufactured in CNC milled molds in a hand-layup technique, including the fitting of fiber optical sensors for strain measurements, Figure 14. After curing the wing skins, in spanwise direction two types of foam were glued in top and bottom half, providing for the larger loads in the wing root by means of a denser foam in this area.

Figure 14: Placement of the strain fiber (left) and a 15° UD glass layer (right)

Second, the sensors listed in Table 3 were installed in the upper and lower half of the wing skins. For that purpose, defined cutouts in the foam core were arranged in combination with tailor-made 3D-printed mounting devices for the various sensor types. Eventually, in step three the model was closed by adhering upper and lower skin.
In a dedicated test setup several servo drives for flap actuation were investigated and compared with respect to their dynamic behavior, eventually resulting in the selection of the "MKS HBL990" brushless digital servo, [26].
Throughout the manufacturing process, all relevant masses, structural and non-structural were exactly measured and tabled, serving as an input to the subsequent model update.

Table 3: Sensors installed in the model.

type	position	output
accelerometer	25% chord: x = 62.5 mm y = [300/600/900/1200/1500] mm	acceleration in z
	60% chord: x = 150.0 mm y = [300/600/900/1200/1500] mm	acceleration in z

	x = 62.5 mm y = [900/1500]mm	acceleration in x
3-axes accelerometer	25% chord: x = 62.5 mm y = [200/400/600/900/1200/1500] mm	acceleration in xyz
strain gauge	upper skin: x = [62.5 /150] mm y = [50 / 50] mm	3-axes strain rosette
	lower skin: x = [62.5 /150 / 150] mm y = [50 / 50 / 600] mm	3-axes strain rosette
strain fiber	25% and 60% chord: y = [0 - 1600] mm	strain in fiber direction
potentiometer	installed in hinge line of each flap	flap deflection

4.2 Model Update

With the aeroelastic model constituting one of the main inputs to the controller design and the resulting actuator excitation driven by the control algorithm, an accurate representation of the aeroelastic model in the simulation is of great importance. Therefore, a finite element model update was performed based on a dynamic identification of the wind tunnel model. Since not only the wing itself, but also the wing mounting has a great influence on the dynamic behavior, the test was performed with the model being mounted on the actual test stand, Figure 15 (left).

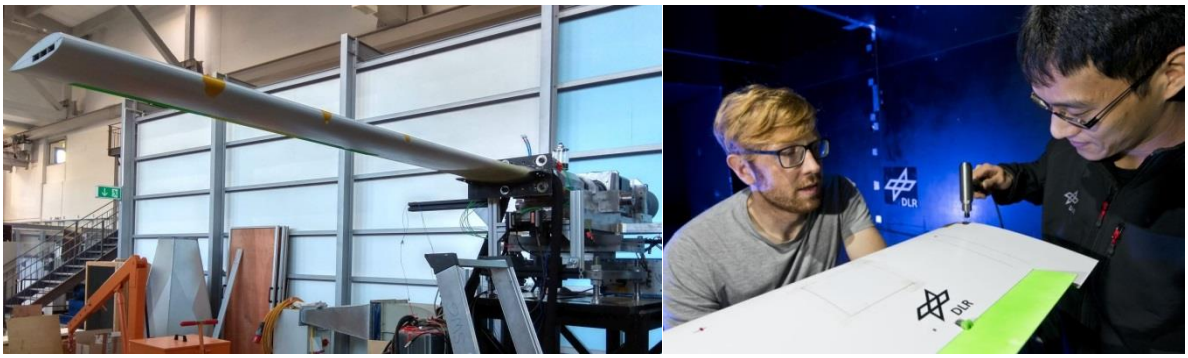

Figure 15: Model mounted on test stand outside the tunnel (left), hammer test inside the tunnel (right).

The identification was conducted with 15 externally installed accelerometers, 13 of which pointed in z-direction (out-of-plane) and 2 in x-direction (in-plane). Eigenfrequencies, mode shapes, modal damping and modal mass were identified by hammer testing, Figure 15 (right).

Table 4: Eigenfrequency comparison.

Mode	measurement	initial FEM	updated FEM
1st wing bending	6.9 Hz	6.2 Hz	6.8 Hz
1st inplane	26.8 Hz	31.4 Hz	36.1 Hz
2nd wing bending	39.0 Hz	39.0 Hz	39.1 Hz
1st torsion	75.2 Hz	69.8 Hz	75.1 Hz

After enhancing the finite element model with the masses identified during the manufacturing process, a model update based on the identified eigenfrequencies could be performed. The resulting eigenfrequencies are listed in Table 4, noting that the initial finite element eigenfrequencies can also be found in Figure 11.

The manual model update was achieved by first identifying the driving parameters which had the largest influence on the eigenfrequencies. It is important to note that only physically meaningful changes were made rather than arbitrary changes of stiffness and weight properties. Eventually, only very minor changes were required to achieve a good agreement between measured and computed eigenfrequencies of the first two bending and the torsional mode:

- between 1° and 2° adaption of the fiber angles in the 15° and -30° wing skin layers (compare Figure 10), owing to uncertainties in the hand-layup
- adaption of a diminution factor accounting for fiber ondulation in the UD glass fiber layer from 0.9 to 1.0 (→ no ondulation effect)
- foam core density reduction, resulting from varying declarations by the manufacturer

The first four mode shapes of the updated finite element model are shown in Figure 16.
Still a large deviation in the 1st inplane mode eigenfrequency persisted, noting however that its contribution to the control algorithms was negligible anyway.

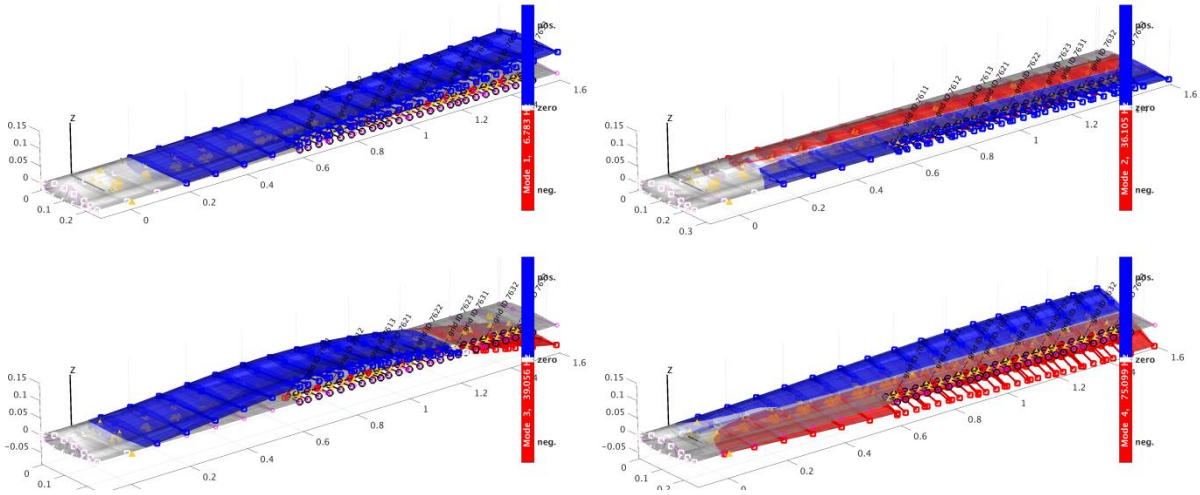

Figure 16: Mode shapes of the updated finite element model.

5 CONCLUSION AND OUTLOOK

The entire process of designing, building and updating a wind tunnel model was presented in this paper. Starting with the general wing layout, complying with the requirements and goals pursued in the project, basic dimensions and aerodynamic parameters were defined. In order to evaluate the most promising combination of passive and active load alleviation means, various combinations of structural optimization and controller design were investigated. Deciding for the wing tailored for aileron effectiveness maximization, the wing was built, followed by an update of the finite element model. The wing was tested in a wind tunnel campaign in November 2018, first results of which were presented in [26].

The experience gained with respect to model optimization, manufacturing aspects, in particular concerning actuated flaps, but also regarding model mounting, will serve as a valuable input for future test campaigns.

6 REFERENCES

[1] W. Krüger, „KonTeKst - Konfigurationen und Technologien für das emissions- und lärmarme Kurzstreckenflugzeug," Göttingen, 2015.

[2] J. H. Starnes Jr und R. T. Haftka, „Preliminary Design of Composite Wings for Buckling, Strength, and Displacement Constraints," *Journal of Aircraft,* Bd. 16, Nr. 8, pp. 564-570, 1979.

[3] S. J. Hollowell und J. Dungundji, „Aeroelastic Flutter and Divergence of Stiffness Coupled, Graphite Epoxy Cantilevered Plates," *Journal of Aircraft,* Bd. 21, Nr. 1, pp. 69-76, 1984.

[4] J. A. Green, „Aeroelastic tailoring of aft-swept high-aspect-ratio composite wings," *Journal of Aircraft,* Bd. 24, Nr. 11, pp. 812-819, 1987.

[5] M. H. Shirk, T. J. Hertz und T. A. Weisshaar, „Aeroelastic tailoring - Theory, practice, and promise," *Journal of Aircraft,* Bd. 23, Nr. 1, pp. 6-18, 1986.

[6] G. N. Vanderplaats und T. A. Weisshaar, „Optimum design of composite structures," *International Journal for Numerical Methods in Engineering,* Bd. 27, Nr. 2, pp. 437-448, 1989.

[7] O. Stodieck, J. E. Cooper und P. M. Weaver, „Interpretation of Bending/Torsion Coupling for Swept, Nonhomogenous Wings," *Journal of Aircraft,* Bd. 53, Nr. 4, 2016.

[8] O. Stodieck, J. E. Cooper, P. M. Weaver und P. Kealy, „Aeroelastic Tailoring of a Representative Wing Box Using Tow-Steered Composites," *AIAA Journal,* Bd. 55, Nr. 4, 2017.

[9] O. Stodieck, J. E. Cooper, P. M. Weaver und P. Kealy, „Improved aeroelastic tailoring using tow-steered composites," *Composite Structures,* Bd. 106, Nr. 0, pp. 703-715, 12 2013.

[10] B. K. Stanford, C. V. Jutte und C. A. Coker, „Aeroelastic Sizing and Layout Design of a Wingbox Through Nested Optimization," *AIAA Journal,* pp. 1-10, 27 12 2018.

[11] C. Jutte und B. K. Stanford, „Aeroelastic Tailoring of Transport Aircraft Wings: State-of-the-Art and Potential Enabling Technologies," Hampton, VA, United States, 2014.

[12] J. K. S. Dillinger, T. Klimmek, M. M. Abdalla und Z. Gürdal, „Stiffness Optimization of Composite Wings with Aeroelastic Constraints," *Journal of Aircraft,* Bd. 50, Nr. 4, pp. 1159-1168, 25 6 2013.

[13] J. Dillinger, „Static Aeroelastic Optimization of Composite Wings with Variable Stiffness Laminates," TU Delft, Delft University of Technology, 2014.

[14] C. D. Regan und C. V. Jutte, „Survey of applications of active control technology for gust alleviation and new challenges for lighter-weight aircraft," NASA, 2012.

[15] T. E. Disney, „The C-5A Active Load Alleviation System," American Institute of Aeroenautics and Astronautics, 1975.

[16] M. Pusch und A. a. K. T. Knoblach, „Integrated Optimization of Ailerons for Active Gust Load Alleviation," in *Internetional Forum on Aeroelasticity and Structural Dynamics (IFASD),* St. Petersburg, Russia, 2015.

[17] M. Pusch, „Allocation of Distributed Flaps for Gust Load Alleviation,“ in *Conference on Control Technology and Application (CCTA)*, Kohala Coast, HI, USA, 2017.

[18] N. Nguyen und J. Urnes, „Aeroelastic Modeling of Elastically Shaped Aircraft Conceptual Wing Shaping Control for Drag Reduction,“ in *AIAA Atmospheric Flight Mechanics conference*, Minneapolis, USA, 2012.

[19] B. Danowsky, P. Thompson und D. Lee, „Modal Isolation and Damping for Adaptive Aeroservoelastic Suppression,“ in *AIAA Atmospheric Flight Mechanics Conference*, Boston, MA, USA, 2013.

[20] M. Pusch, „Aeroelastic Mode Control using H2-optimal Blends for Inputs and Outputs,“ in *2018 AIAA Guidance, Navigation, and Control Conference*, American Institute of Aeronautics and Astronautics, 2018.

[21] Y. Meddaikar, J. Dillinger, J. Sodja, H. Mai und R. de Breuker, „Optimization, manufacturing and testing of a composite wing with maximized tip deflection,“ in *57th AIAA/ASCE/AHS/ASC Structures, Structural Dynamics, and Materials Conference*, 2015.

[22] M. Y. Meddaikar, J. Dillinger, M. R. Ritter und Y. Govers, „Optimization & Testing of Aeroelastically-Tailored Forward Swept Wings,“ in *IFASD 2017 - International Forum on Aeroelasticity and Structural Dynamics*, 2017.

[23] T. Klimmek, „Parameterization of topology and geometry for the multidisciplinary optimization of wing structures,“ in *CEAS 2009 - European Air and Space Conference*, Manchester, UK, 2009.

[24] E. Ferede und M. Abdalla, „Cross-sectional modelling of thin-walled composite beams,“ in *55th AIAA/ASME/ASCE/AHS/ASC Structures, Structural Dynamics, and Materials Conference*, p. .

[25] Y. Meddaikar, F.-X. Irisarri und M. Abdalla, „Blended Composite Optimization combining Stacking Sequence Tables and a Modified Shepard's Method,“ in *{11th World Congress on Structural and Multidisciplinary Optimization (Submitted)}*, Sydney, Australia, 2015.

[26] M. Pusch, D. Ossmann, T. Kier, M. Tang, J. Lübker und D. J., „Aeroelastic Modeling and Control of an Experimental Flexible Wing,“ in *Guidance, Navigation and Control (GNC), AIAA SciTech*, San Diego, USA, 2019.

COPYRIGHT STATEMENT